Fatigue and Corrosion Fatigue Properties of Ti-6Al-4V Implant Grade Titanium Alloy in Ringer Solution

Saeid Yazdani, Mahmoud Hajisafari*, Arman Zare Bidaki

Department of Metallurgy and Materials Engineering, Yazd Branch, Islamic Azad University, Yazd, Iran.

ARTICLE INFO

Article history:

Received 10 June 2017
Accepted 29 August 2017
Available online 15 December 2017

Keywords:

Ti-6Al-4V alloy
Corrosion fatigue Microstructure
Fracture surface
Striation features

ABSTRACT

Nowadays, modification of metallic biomaterials which are used as implants for bone and hard tissues replacement is considered as an important subject. In the current study, corrosion fatigue properties of the Ti-6Al-4V alloy were investigated via Rotating-Bending standard test method and then the results were compared with the fatigue properties of the specimens tested in the same conditions. Scanning electron microscopy (SEM) was used to investigate the chemical composition (EDS- Energy-dispersive X-ray spectroscopy), microstructural features and crack propagation characteristics. The results showed that the presence of corrosive environment not only results in the decrease in the fatigue life, but also eliminates the fatigue limit. Further studies revealed that aggregation of the corrosion products with more hardness values at the crack tip will cause an obvious deviation of crack propagation from its main direction. Therefore, a tortuous crack path through the bulk of the specimens was detected concurrent with penetration of solution into the crack. In addition, dimensions and morphology of fatigue crack surfaces were completely different from corrosion fatigue cracks.

1-Introduction

Metallic biomaterials are still extensively used for the reconstruction of failed hard tissues such as bone. Modification of such metallic biomaterials (involving mechanical modification) is becoming the most important issue in the development of high performance metallic biomaterials for the manufacturing of implant devices [1]. In other words, for any material to be used as implant, it needs to fulfil different requirements such as mechanical, electrochemical, and biological [2]. Mechanical properties of titanium alloys usually depend on morphology, volume fraction and properties of both α and β phases. The limitations in strength that can be developed in the fully-α alloys because of the ordering reaction occurring at higher solute contents, together with difficulties with hot-forming, led to the early investigation of compositions containing both the α- and β-phases. These α/β alloys now have the greatest commercial importance with one composition, Ti–6Al–4V (IMI 318)[3]. A group of researchers focused on the influence of effective foreign parameters on fatigue life of titanium alloys. For instance, the effect of Foreign Object Damage (FOD) on the fatigue behavior of Ti-6Al-4V alloy was examined by Peters et al. [4]. Their results showed that FOD impact of steel spheres on flat surface markedly degraded resistance to high-cycle fatigue.

On the other hand, the results obtained by

* Corresponding author:
E-mail address: hajisafari1001@iauyazd.ac.ir

different researches on various titanium alloys and commercially pure titanium (CpTi) revealed significant decrease in fatigue life of the samples in various saline solutions including simulated body fluid (SBF) in comparison with similar experiments in air at room temperature [5-7]. Azevedo et al. [8] showed that the fatigue life of CpTi plates tested in serum at 37°C, decreased when compared with a similar test in air. Akahori et al. [9] investigated plain and fretting fatigue properties of β type titanium alloy, Ti-29Nb-13Ta-4.6Zr (TNTZ), in air and Ringer solution which experienced different thermo-mechanical treatments. They found that the fatigue strength of both the solutionized and aged samples was same in the aforementioned environments. At the same time, Baptista et al. [10] studied the fatigue behavior of Ti-13Nb-13Zr titanium β type alloy. Their results showed that the alloy is not sensitive to the environment therefore the curves obtained in air and in the saline solution were the same. Boehlert et al. [11] have also demonstrated such insensitivity for other β type titanium alloys. Based on these results, Majumdar et al. [12] ignored the evaluation of the fatigue behavior of Ti–13Nb–13Zr and Ti–13Nb–13Zr–0.5B in SBFs, performing the fatigue tests only in air.

Considering the particular role of Ti-6Al-4V titanium alloy as a high performance metallic biomaterial for in vivo situations, and also the lack of information about its corrosion fatigue properties in such environments, the aim of this study is to investigate the corrosion fatigue properties of the aforementioned alloy in Ringer solution using standard Rotating-Bending method. For comparative purpose, the same measurements were also performed on similar Ti-6Al-4V titanium samples in air using the same stress levels.

2-Experimental procedure

2-1-Materials

In order to prepare the samples, annealed Ti-6Al-4V titanium alloy rods (LOTERIOS, Italy) with nominal diameter of 10 mm were used. The chemical composition of the samples (presented in Table 1) was analyzed using Optical Emission Spectroscopy (OES) method (OXFORD- FOUNDRY MASTER PRO 2013). The tensile properties and hardness of samples investigated by uniaxial tensile testing method (GOTECH) and micro hardness test (Future-Tech FM-700), respectively, are listed in Table 2.

Table 1. Chemical composition of Ti-6Al-4V titanium alloy.

Element	Al	V	Fe	Cu	Ni	Si	Zr	Ti
(Wt. %)	6.3	4.35	0.03	0.02	0.005	0.02	0.01	Balance

Table 2. Mechanical properties of Ti-6Al-4V titanium alloy.

Tensile Strength	Yield Strength 0.2%	Elongation	Area of reduction	Hardness Average
940 MPa	870 MPa	16%	48%	36 HRC

Titanium rods were machined using a CNC lathe in accordance with ASTM F1801 standard [13] necessities (Fig. 1). In order to minimize the surface residual stress throughout the machining procedure, a very strong control was performed on the machining procedure concurrent with sample cooling.

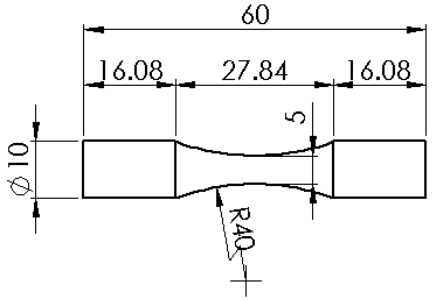

Fig. 1. Shape and test specimen dimensions (mm).

In the next step, to obtain the desired specimens gauge area surface quality, the polishing process was performed on the previously mentioned surface of all samples using silicon carbide papers No. 1000, 1500, 2000, 2500 and 3000. However, the polishing steps were followed by using polishing paste and finally cotton to avoid notch effects and surface grooves. Furthermore, in accordance with ASTM F1801 necessities, all mechanically finished specimens were degreased in acetone, flushed with ethyl alcohol, then with distilled water, and finally blown dried with warm air [13].

2-2-Fatigue and corrosion fatigue testing

Standard Rotating-Bending fatigue tests in air were performed using fatigue testing machine on three groups of samples in accordance with

ASTM E466 [14] necessities and the obtained results were reported as Fatigue Test Group No. 1 to 3 (Fig. 2, Curve A shows the average of the obtained values in air). Similarly, corrosion fatigue tests in Ringer solution were accomplished using corrosion fatigue testing machine on three groups of samples in accordance with ASTM F1801 [13] necessities and the obtained results were reported as Corrosion Fatigue Group No. 1 to 3 (Fig. 2, Curve B also shows the average of the obtained values in Ringer solution).

In both tests, a sinusoidal cyclic waveform with cycling frequency of 1.0 Hz [13] and a load ratio R=-1 were adopted and for each stress level three identical samples were tested and the average of the obtained values, related to No. of cycles to failure, used for S-N curve preparation. In addition, in corrosion fatigue tests, to simulate human body fluid, each sample was exposed to a minimum of 1000 mL of Ringer solution per square centimeter of specimen surface (6 Liters per each specimen) while the electrolyte was charged to the reservoir recirculating with adequate low flow rate. The pH value was continuously monitored and controlled carefully to stay within the range of 7.30±0.1 throughout the tests. Also, the solution temperature was adjusted to the range of 37±1˚C which was monitored continually with the accuracy of 0.1˚C throughout the tests. Furthermore, in order to minimize the chance of galvanic corrosion between the sample and sample holders, both ends of the selected sample were insulated with inelastic insulator prior to the start of each test. Moreover, the specimens were exposed to the liquid environment 2 hours before the start of loading. Stress levels of cyclic loading, in both fatigue and corrosion fatigue tests, started at $\frac{2}{3}\sigma_{UTS}$ (ultimate tensile strength, 630 MPa) and finished at approximately $\frac{1}{2}\sigma_{UTS}$ (470 MPa).

The specimens fracture surfaces were examined using field emission scanning electron microscopy (FESEM, MIRA3 TESCAN) equipped with energy-dispersive X-ray spectroscopy (EDS) and back scattered electron detector. Additionally, MIP4 software (Microstructural Image Processing) was used for SEM (Scanning Electron Microscopy) micrographs analysis.

3-Results and discussion

3-1-Fatigue and corrosion fatigue properties

The S-N curve (Stress-Average of Number of cycles to failure) of Ti-6Al-4V titanium alloy related to fatigue and corrosion fatigue tests are shown in Fig. 2 as curve A and B, respectively. As can be seen in Fig. 2A, the tested samples have the fatigue limit and fatigue life equal to 490 MPa and 1.2×10^7 cycles, respectively. On the other hand, although the tests were continued to stress level of 450 MPa, the results obtained from corrosion fatigue tests revealed that the presence of corrosive environment not only results in considerable decrease in the fatigue life of the alloy, but also eliminates the fatigue limit. Some researchers [5] believe that in laboratory experiments design step, the role of aggressive environments and its effect on specimens should be considered. So, considering the fracture surface morphology of corrosion fatigue samples and reduction in the number of cycles to failure would be accounted as a result of corrosion or superficial reactions [7] of material embrittlement [6]. Moreover, at the stresses above the fatigue limit in air, the loss of fatigue resistance in SBF is attributed to the mechanical breakdown of the protective film [15]. Therefore, the findings of this study are in line with reference [5].

The corrosion fatigue fracture surface of a sample after 2.61×10^6 cycles is shown in Fig. 3a. As can be clearly observed, the fatigue fracture zone decreases significantly compared to the fatigue surface fracture in air (Fig. 3b). Furthermore, at the peripheral zone of final fracture area, a sharp edge has been created which extends considerably compared to the corresponding area of fatigue test fracture surface in air. The reason of both aforementioned cases is attributed to the fatigue life loss of corrosion fatigue samples due to the variation in fatigue crack propagation behavior.

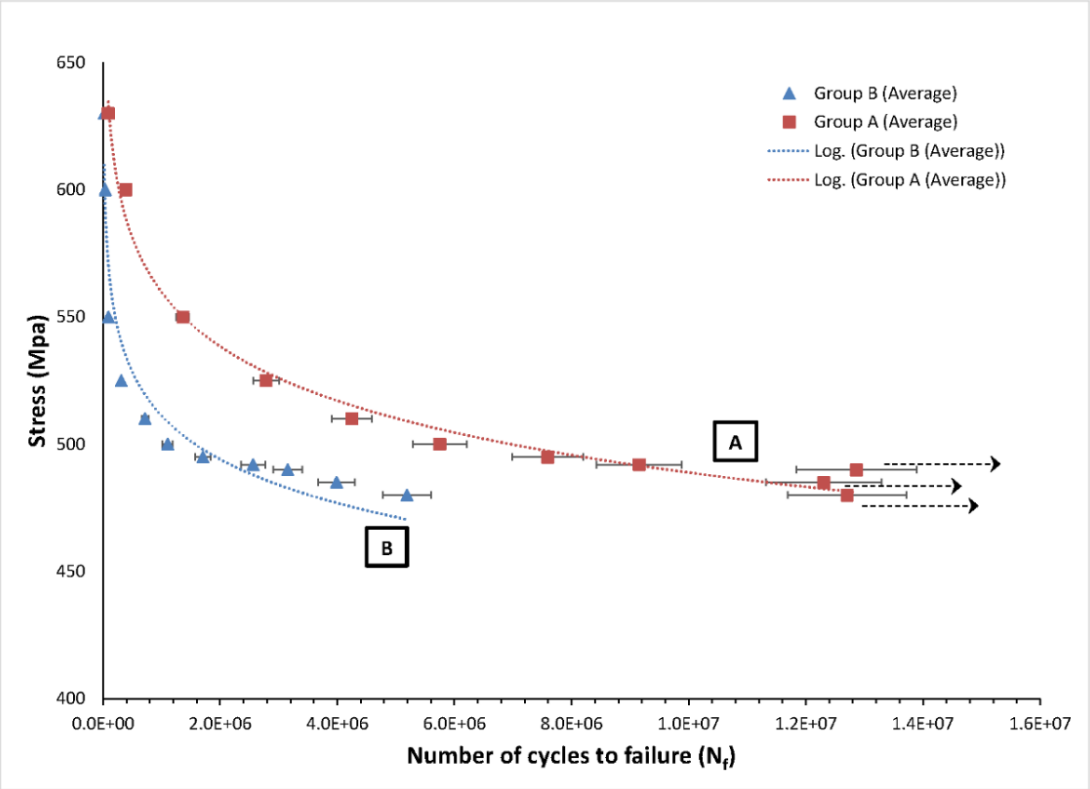

Fig. 2. S-N Curves for Ti-6Al-4V titanium alloy: (A) In air. The arrows represent failure did not occur after 10^7 cycles, (B) In Ringer solution.

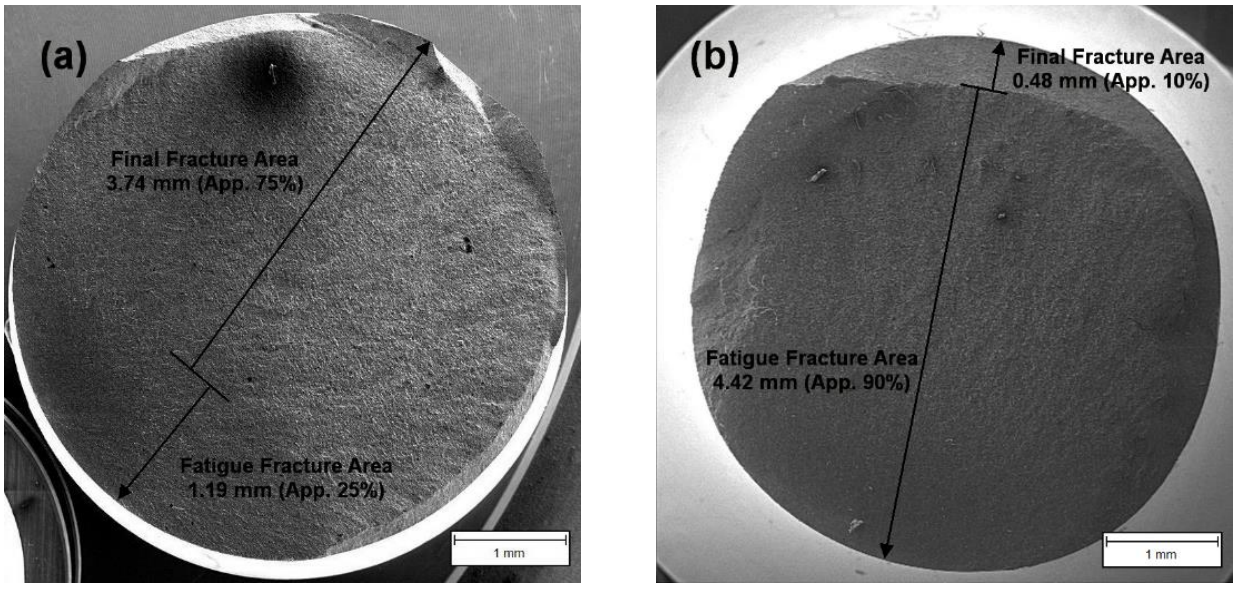

Fig. 3. Samples Fracture surface: (a) Corrosion fatigue fracture surface (applied stress 492 MPa and fatigue life 2.61×10^6 cycles), and (b) Fatigue fracture surface in air (applied stress 492 MPa and fatigue life 9×10^6 cycles).

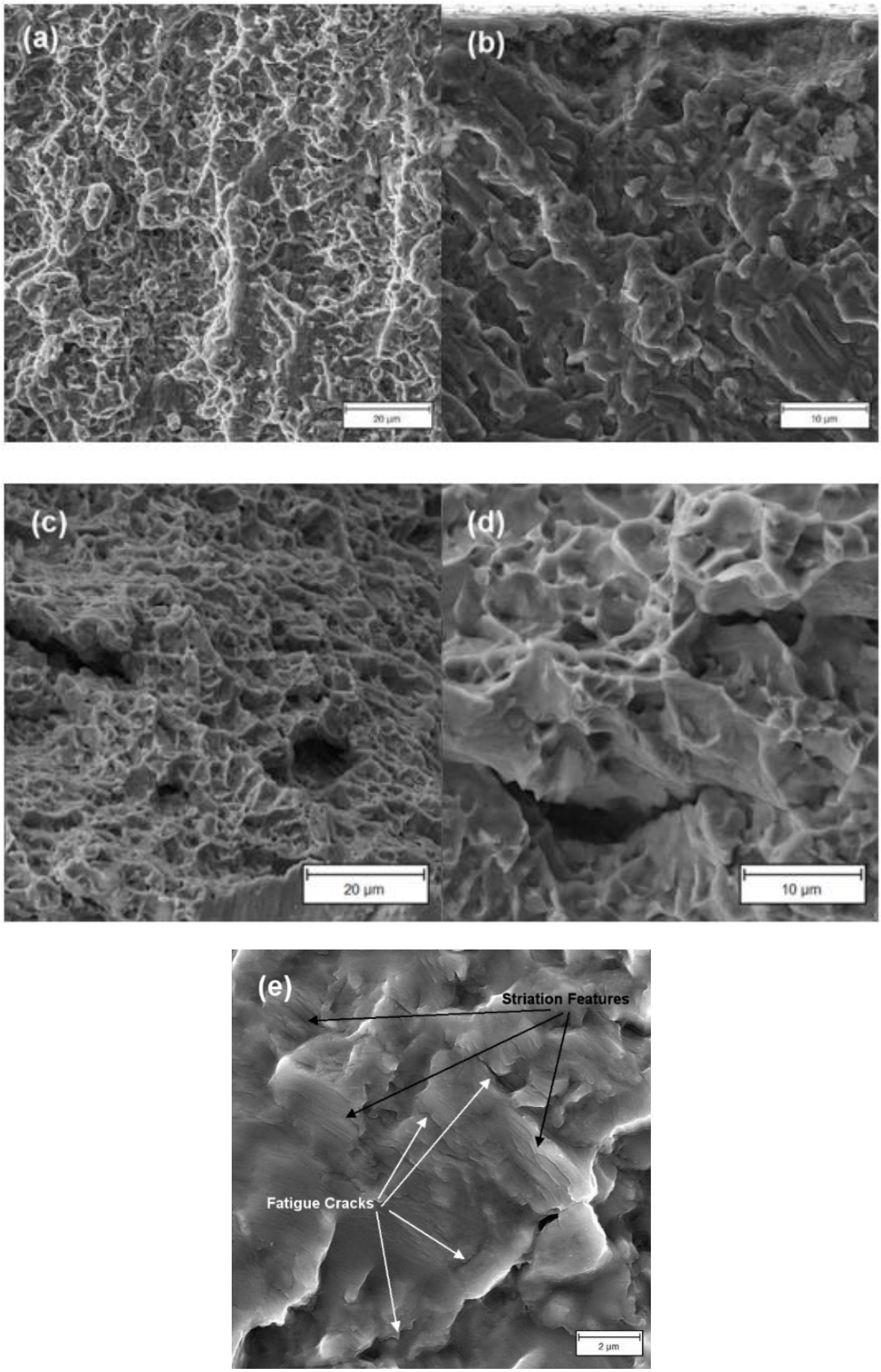

Fig. 4. Fatigue fracture surface: (a) and (b) in Ringer's solution (FESEM), (c) and (d) in air (SEM) and (e) Striation features and fatigue cracks in Ringer solution (FESEM magnification: 15 kx).

FESEM images of fracture surface in Ringer solution are shown in Fig. 4a, b and e and SEM images of mentioned surface in air are also shown in Fig. 4c and d in different scales. The striation features which are created by cyclic loading beside the cracks in corrosion fatigue area are clearly observable (Fig. 4e). Moreover, an important point in the aforementioned images (especially Fig. 4e) is that unlike the fracture surface of in air tested samples, there is no observable fatigue cracks in the fracture surface of the corrosion fatigue samples in low magnifications. However, at higher magnifications micro cracks can be seen through the surface. An example of these kinds of cracks is shown in Fig. 5. These cracks are scattered through the samples fatigue fracture area. The changes in size and crack propagation behavior can be attributed to the corrosion phenomenon so that a fatigue crack is faced to a corrosion product with a higher hardness value compared to the alloy which usually causes the crack to deviate from its main direction.

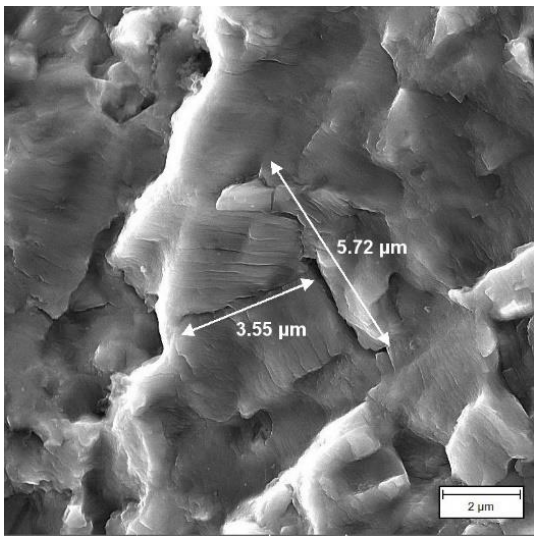

Fig. 5. Typical fatigue cracks and their dimensions.

In Fig. 6 the distance between striation feature lines of both fatigue and corrosion fatigue samples can be compared. The images clearly show that in the abovementioned testing sample, the distance of corrosion fatigue in Ringer solution (Fig. 6a) is approximately 30% of the distance between striation lines of the samples which were tested in air (Fig. 6b). This is attributed to the presence of aggressive environment surrounding the fracture surface throughout the cyclic loading. The occurrence of corrosion on fracture surface caused surface grooves height reduction and, as a result, the distance between two vicinal peaks decreased.

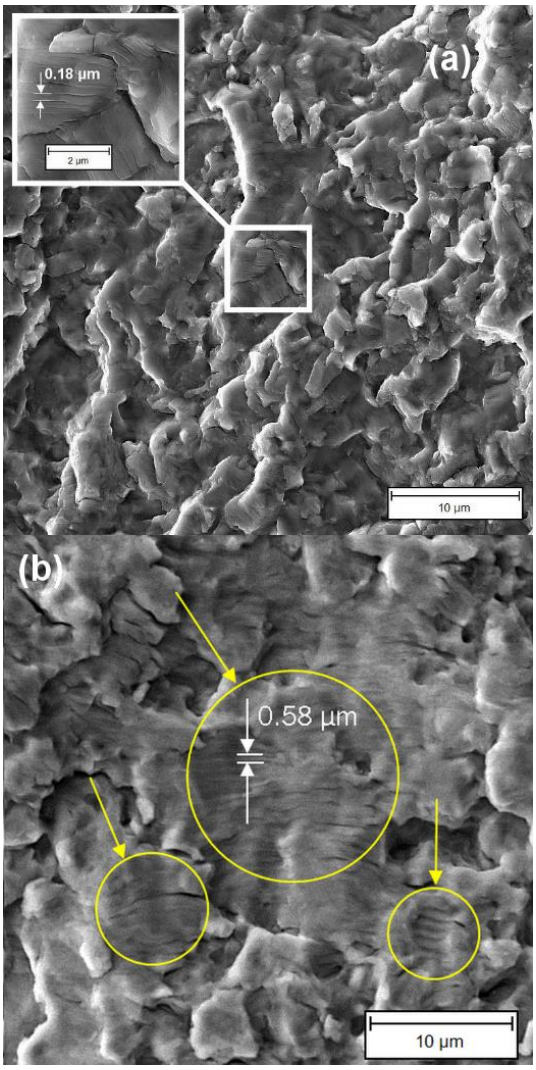

Fig. 6. Striation features: (a) corrosion fatigue fracture surface in Ringer's solution, and (b) fatigue fracture surface in air.

Another important point about the fracture surface is its stepped feature; there are obvious stepped-form wrinkles detectable throughout the crack propagation direction. Fig. 7 shows how cracks propagate among the fracture surface. This behavior can be explained by the synchronization of corrosion phenomenon with cyclic loading. That is, concurrent with crack growth, corrosion causes considerable aggregation of corrosion products (usually having more hardness values) at the crack tip. Aggregation of these compounds makes the crack deviate from its main direction and, as a result, the corrosion proceeds concurrently with cyclic loading causing the surface to form a

step. Then, the crack continues its propagation from the beginning of the "formed step". It is noticeable that this behavior is not observed on the fatigue fracture surface in air.

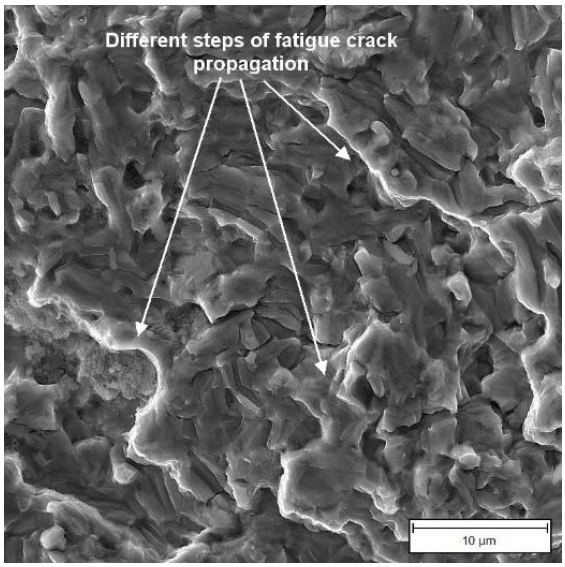

Fig. 7. Steps formed on the corrosion fatigue surface.

Additional investigations on the hollow spots located in circumference of fracture surface (Fig. 8) revealed that in some sites, slight effects of striation features are observable whose presence implies the contribution of both fatigue and cyclic loading on forming the hollow spots. As a result, these hollows are the first step of fatigue cracks growth. Like fatigue test in air, cracks nucleate from the intrusions or pultrusions of sample surface in gauge area. Compared to other areas of fracture surface, due to the rather long duration of surface immersion in aggressive environment, more volume of corrosion products were aggregated there. Furthermore, not only the first step area is less extended (because of the quickly formed corrosion products presented at crack tip), but also the fatigue marks (micro cracks and striation features) are faded due to corrosion persistence. Although these sites are almost not extended, they can be the origin of crack re-nucleation (Fig. 8b). Additional investigations on cracks shown in Fig. 8b were performed. The first step of crack nucleation and propagation from the beginning of mentioned step were studied carefully using higher magnifications (Fig. 9).

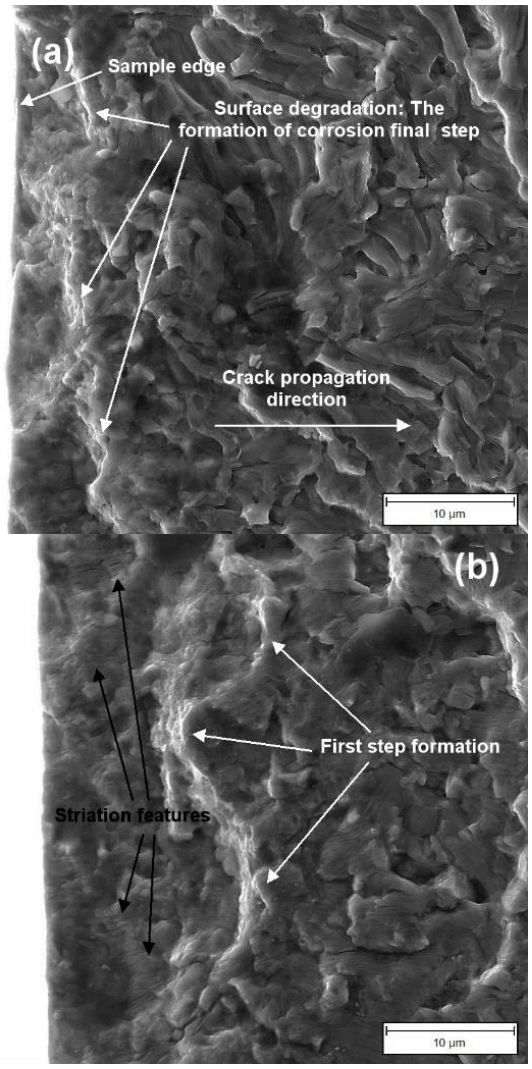

Fig. 8. First step formation: (a) Crack propagation and first step surface dimension, (b) Fatigue marks.

As can be seen, crack propagation started at the beginning (Points A, B, C and D) and continued throughout this step. Also, similar to the previous step, due to the synchronized fatigue and corrosion phenomena on this surface, and because of the penetration of aggressive medium (Ringer's Solution) into the crack tip during the cyclic loading application on the sample, both corrosion and fatigue footprint are clearly observable in the form of micro cracks and stepped featured surface. Generally, the interaction between these two factors (corrosion and cyclic loading) caused the samples to experience failure.

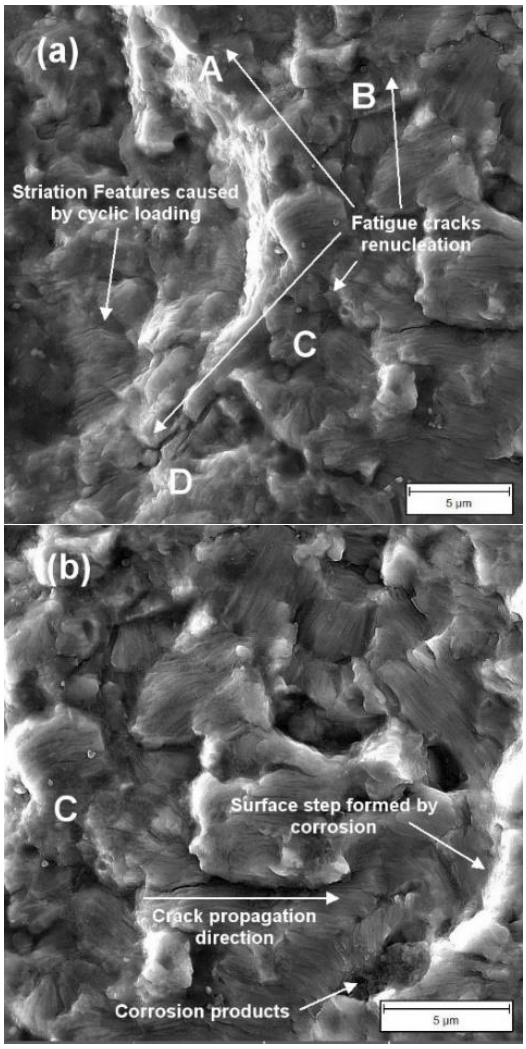

Fig. 9. Steps on fracture surface: (a) crack nucleation at the beginning of step on points A to D (FESEM magnification: 8 kx), and (b) crack propagation from point C and its direction (FESEM magnification: 10 kx).

Further studies were carried out on corrosion product compounds using EDS on different selected points for the purpose of detailed investigation. Images of corrosion-produced compounds formed on fracture surface and their energy-dispersive X-ray spectra are shown in Fig.10. Also, the average of chemical composition on this surface (points A to C of Fig. 10) is listed in Table 3. According to the Table, the remained compounds on fracture surface are mainly formed by Potassium, Calcium, Oxygen, Magnesium, silicon and the alloy elements so that they can be considered as the corrosion products.

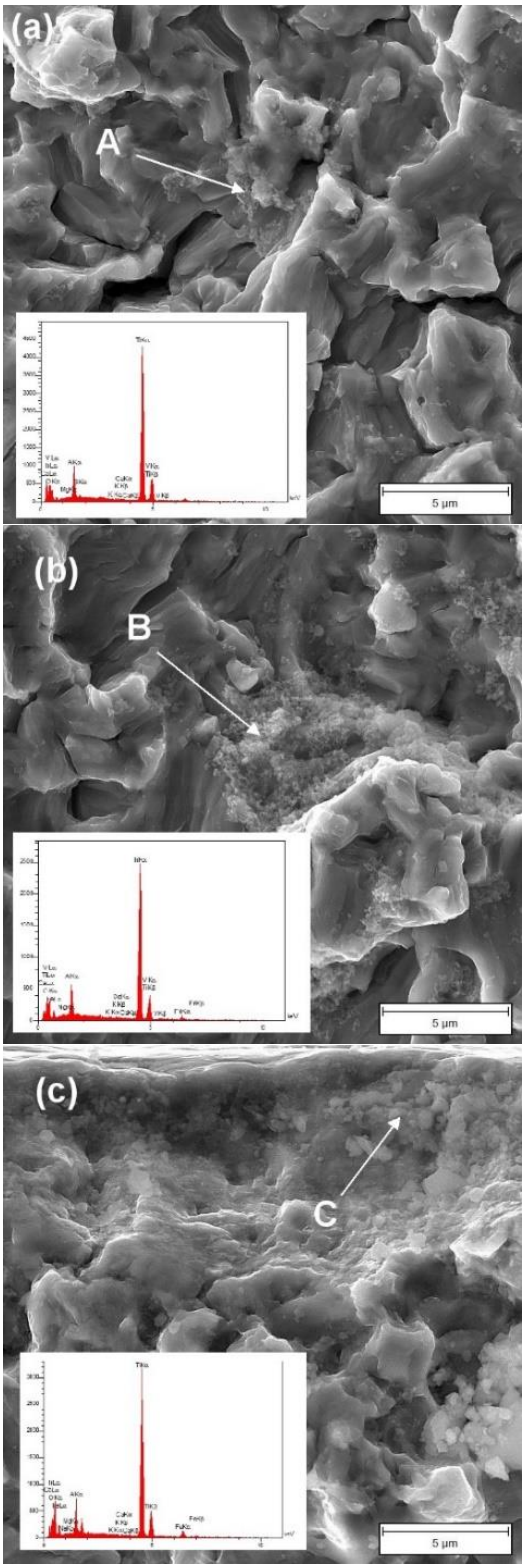

Fig. 10. Remained corrosion products on fracture surface: (a) and (b) corrosion products formed at the end of each step and (c) corrosion products formed on the first step

Table 3. Average of chemical composition analysis (points A to C of Fig. 10).

Element	O	Mg	K	Ca	Al	V	Ti
Content(%wt)	22.42	0.16	0.04	0.09	5.79	1.8	69.67

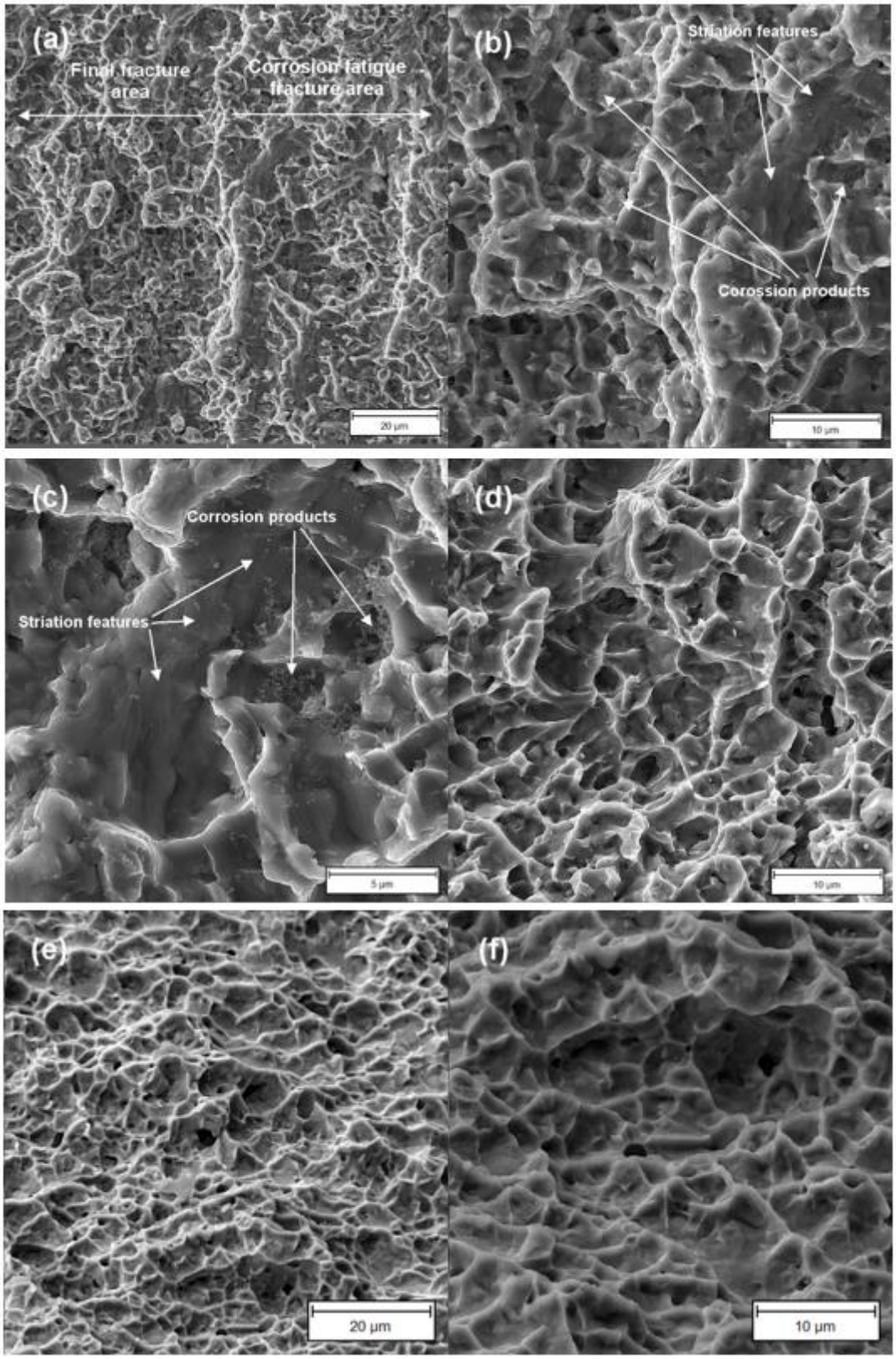

Fig. 11. The corrosion fatigue and final fracture boundary: (a) boundary in Ringer's solution (Magnification: 2 kx), (b) and (c) existence of striation features and corrosion products in fatigue fracture surface in Ringer's solution, (d) final fracture area Ringer's solution (Magnification: 5 kx), (e) final fracture in air (Magnification: 2 kx), and (f) final fracture in air (Magnification: 4 kx).

The boundary between corrosion fatigue area and final fracture is shown in Fig. 11 with different magnifications. As can be seen in Fig. 11a to Fig. 11c, the footprint of both striation features and corrosion products are simply observable, whereas comparing the final fracture area (Fig. 11d) with the images of fatigue tested sample in air (Fig. 11e and 11F) FESEM image of the peripheral sharp edge on the final fracture area is presented in Fig. 12. As can be seen, although the fracture behavior of sample in this area is considered to be ductile fracture, it seems that due to both thickness reduction (caused by extensive crack propagation) and sample inability to tolerate the applied loading, a catastrophic fracture occurred parallel to the surface damage formation. The effects of this stage are clearly evident as surface peeling and distortions.

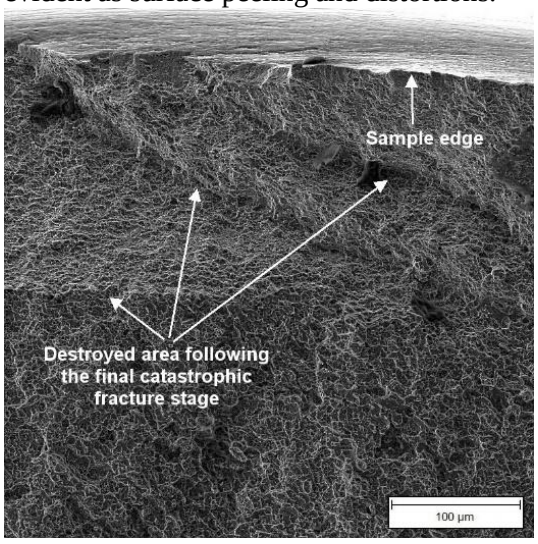

Fig. 12. Damaged surface caused by the final catastrophic fracture

4-Conclusion

In this paper, corrosion fatigue properties of Ti-6Al-4V titanium alloy samples were investigated in Ringer solution and the results were compared to the data provided by similar tests in air. The main conclusions of this study are as follows:

1) The presence of corrosive environment not only results in considerable decrease in the fatigue life of the alloy (from 1.2×10^7 cycles to 3.2×10^6 cycles in air), but also eliminates the fatigue limit (490 MPa in air).
2) The appearance of fatigue cracks in the corrosion fatigue test completely differs from the air tested fatigue crack. This difference is clearly observable in both crack dimensions and crack propagation reveals that the appearance of the corrosion fatigue fracture surface dimples are different from that of fatigue test in air. In other words, considering the appearance of this area, the alloy behavior can be attributed to a mixture of ductile and brittle fracture. However, the ductile fracture behavior seems to be the main fracture behavior.

behavior.

3) The presence of corrosive media and its penetration to the crack tip causes a significant destroy on fracture surface and remained fatigue footprints.
4) Synchronization of corrosion with cyclic loading caused a considerable decrease in the proportion of fatigue fracture area by final fracture area.
5) The final fracture of corrosion fatigue samples was a mixture of brittle and ductile fracture.
6) Although the Ti-6Al-4V titanium alloy has an almost high corrosion resistance in Ringer solution, the corrosion footprints are observable on the fracture surface as surface steps.
7) Aggregation of the corrosion-produced compounds at crack tip results in an obvious deviation in crack propagation from its main direction and propagation process will be followed by a tortuous path through the bulk of the specimens.

References

[1] M. Niinomi, A. Saga, and K.-i. Fukunaga, "Long crack growth behavior of implant material Ti–5Al–2.5Fe in air and simulated body environment related to microstructure", International Journal of Fatigue, vol. 22,2000,pp. 887-897

[2] R. K. Singh Raman, S. Jafari, and S. E. Harandi, "Corrosion fatigue fracture of magnesium alloys in bioimplant applications: A review", Engineering Fracture Mechanics, vol. 137,2015,pp. 97-108

[3] I. J. Polmear, *Light Alloys*. Oxford: Butterworth-Heinemann, 2005.

[4] J. O. Peters and R. O. Ritchie, "Influence of foreign-object damage on crack initiation and early crack growth during high-cycle fatigue of Ti–6Al–4V", Engineering Fracture Mechanics, vol. 67,2000,pp. 193-207

[5] M. R. Bache and W. J. Evans, "The fatigue crack propagation resistance of Ti–6Al–4V under aqueous saline environments", International Journal of Fatigue, vol. 23,

Supplement 1,2001,pp. 319-323
[6] M. Papakyriacou, H. Mayer, C. Pypen, H. Plenk Jr, and S. Stanzl-Tschegg, "Effects of surface treatments on high cycle corrosion fatigue of metallic implant materials", International Journal of Fatigue, vol. 22,2000,pp. 873-886
[7] R. A. Zavanelli, P. Henriques, I. Ferreira, and J. M. D. d. Almeida Rollo, "Corrosion-fatigue life of commercially pure titanium and Ti-6Al-4V alloys in different storage environments", Journal of Prosthetic Dentistry, vol. 83,2000,pp. 274-279
[8] C. R. F. Azevedo and A. P. dos Santos, "Environmental effects during fatigue testing: fractographic observation of commercially pure titanium plate for cranio-facial fixation", Engineering Failure Analysis, vol. 10,2003,pp. 431-442
[9] T. Akahori, M. Niinomi, H. Fukui, and A. Suzuki, " Fretting Fatigue and Corrosion Characteristics of Biocompatible Beta Type Titanium Alloy Conducted with Various Thermo-Mechanical Treatments", Materials Transactions, vol. 45,2004,pp. 1540-1548
[10] C. A. R. P. Baptista, S. G. Schneider, E. B. Taddei, and H. M. da Silva, "Fatigue behavior of arc melted Ti–13Nb–13Zr alloy", International Journal of Fatigue, vol. 26,2004,pp. 967-973
[11] C. J. Boehlert, C. J. Cowen, C. R. Jaeger, M. Niinomi, and T. Akahori, "Tensile and fatigue evaluation of Ti–15Al–33Nb (at.%) and Ti–21Al–29Nb (at.%) alloys for biomedical applications", Materials Science and Engineering: C, vol. 25,2005,pp. 263-275
[12] P. Majumdar, S. B. Singh, and M. Chakraborty, "Fatigue behaviour of boron free and boron containing heat treated Ti-13Zr-13Nb alloy for biomedical applications", Materials Characterization, vol. 61,2010,pp. 1394-1399
[13] ASTM International, "Standard Practice for Corrosion Fatigue Testing of Metallic Implant Materials," in *13.01: Medical and Surgical Materials and Devices (I): E667 - F2477*, ed. West Conshohocken, 97(2014).
[14] ASTM International, "Standard Practice for Conducting Force Controlled Constant Amplitude Axial Fatigue Tests of Metallic Materials," in *03.01: Metals -- Mechanical Testing; Elevated and Low-Temperature Tests; Metallography*, ed. West Conshohocken, 2015.
[15] S. Jafari, R. K. Singh Raman, and C. H. J. Davies, "Corrosion fatigue of a magnesium alloy in modified simulated body fluid", Engineering Fracture Mechanics, vol. 137,2015,pp. 2-11